CDF Note 8954 v1.0

Search for Higgs Bosons Produced in Association with b-Quarks

The CDF Collaboration

URL http://www-cdf.fnal.gov

(Dated: August 10, 2007)

We present a search for neutral Higgs bosons decaying into $b\bar{b}$, produced in association with b-quarks in $p\bar{p}$ collisions. This process could be observable in supersymmetric models with high values of $\tan\beta$. We search for an enhancment in the mass of the two lead jets in triply b-tagged events, using 980 pb^{-1} of data collected with the CDF II detector at the Fermilab Tevatron collider. The dijet mass spectrum of the heavy flavor multi-jet background is derived from double-tagged data in a manner that accounts for tagging biases and kinematic differences introduced by the addition of the third tag. We set mass-dependent limits on $\sigma \times BR$ and $\tan\beta$ in MSSM models.

Preliminary Results for Summer 2007 Conferences

FIG. 1: MSSM Higgs cross sections for various production modes at $\tan\beta = 40$ in the m_h^{max} scenario, from the TeV4LHC Working Group [2].

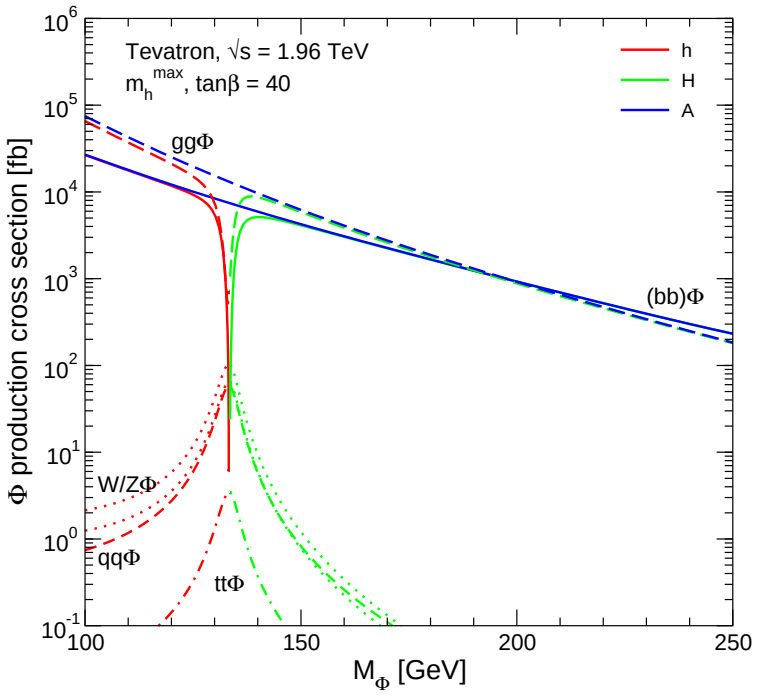

I. INTRODUCTION

The production rate of light Higgs bosons in association with b-quarks can be significantly enhanced in supersymmetric extensions of the standard model. This occurs for large values of $\tan\beta$, the ratio of the Higgs coupling to down-type versus up-type quarks. Figure 1 shows the cross section expected for $\tan\beta = 40$ in the m_h^{max} benchmark scenario [1], from the TeV4LHC Working Group [2]. The cross section for $(bb)\Phi$ is in the 10 pb range, which could potentially be observable at the Tevatron. Also interesting is that at large $\tan\beta$ the pseudoscalar A becomes degenerate with either the light (h) or heavy (H) scalar, giving an effective factor of two enhancement to the cross section.

The cross sections shown in Figure 1 are for inclusive production [3], however only the case where at least of the b's accompanying the Higgs is at high p_T is relevant to these results, since we will require that it be b-tagged. Fortunately, as shown in Figure 2, cross section calculations are available for this case as well [4, 5, 6], allowing for the interpretation of the results of the search described in this note.

Results for the Higgs+1b process in the case of Higgs decays to $b\bar{b}$ have been obtained by DØ [7, 8], and for inclusive Higgs production in the $\tau\tau$ decay mode by CDF [9, 10] and DØ [11, 12, 13].

In this analysis we search for Higgs decays into $b\bar{b}$, accompanied by an additional high-p_T b, giving an event signature of at least three b-jets. We study the dijet mass spectrum of the two leading jets in three-jet events with all three jets identified as b-jet candidates

FIG. 2: MSSM Higgs cross sections at $\tan\beta = 40$ as a function of the number of high-p_T b quarks accompanying the Higgs (taken from Ref. [5]).

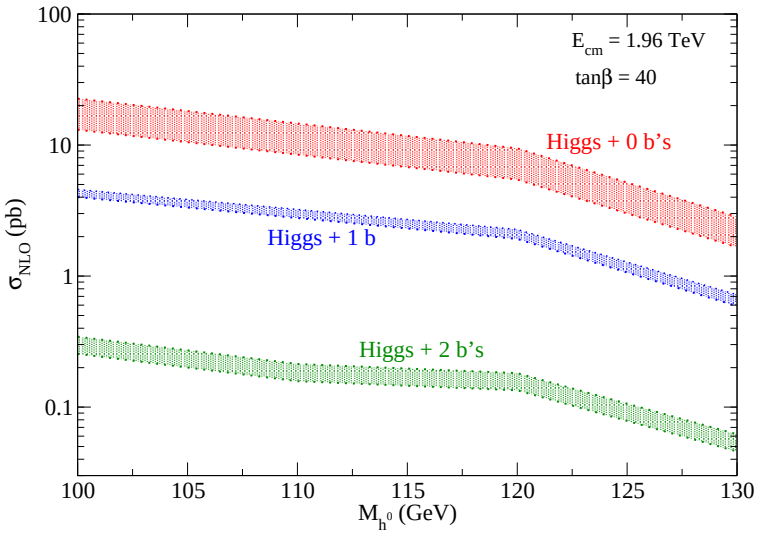

using a displaced vertex algorithm [15]. We use the dijet mass of the two leading jets in the events m_{12} to separate Higgs signal from background events. We also define a quantity $m_{diff} = m_1^{tag} + m_2^{tag} - m_3^{tag}$, where m_i^{tag} is the mass of the tracks forming the displaced vertex in jet 1, 2, or 3. This quantity is sensitive to the flavor composition of the backgrounds.

II. DATA SAMPLE & EVENT SELECTION

This analysis is based on an integrated luminosity of 980 pb^{-1} collected with the CDF II detector [14] between February 2002 and February 2006. The data are collected on a trigger requiring two central energy clusters with $E_T > 15$ GeV and a third cluster with $E_T > 10$ GeV. The 15 GeV clusters are each required to match in ϕ to a track with $p_T > 2$ GeV/c and impact parameter $|d_0| > 120$ μm, reconstructed using the Level2 silicon vertex tracker system.

The offline selection requires three jets with $E_T > 20$ GeV and detector rapidity $|\eta| < 2$. The jets are reconstructed using a cone algorithm with radius $\sqrt{\delta\phi^2 + \delta\eta^2} < 0.7$, and are corrected for calorimeter response and multiple interactions so that the energy scale mirrors the total p_T of all particles within the jet cone. The two leading jets in the event must match to the 15 GeV energy clusters and displaced tracks in the Level2 trigger selection, and the third jet is require to match the additional 10 GeV cluster. All three of the jets must be tagged as b-jets using the SECVTX algorithm [15], which searches for displaced b-decay vertices using the tracks within the jet cone. We also select an auxiliary sample with no SECVTX tag requirement on the third jet which is used for constructing background estimates.

The efficiency of this selection on bH events where the Higgs decays into a $b\bar{b}$ pair is determined from simulated data generated using the PYTHIA [16] Monte Carlo program.

FIG. 3: Selection efficiency for bH events as a function of the Higgs mass m_H.

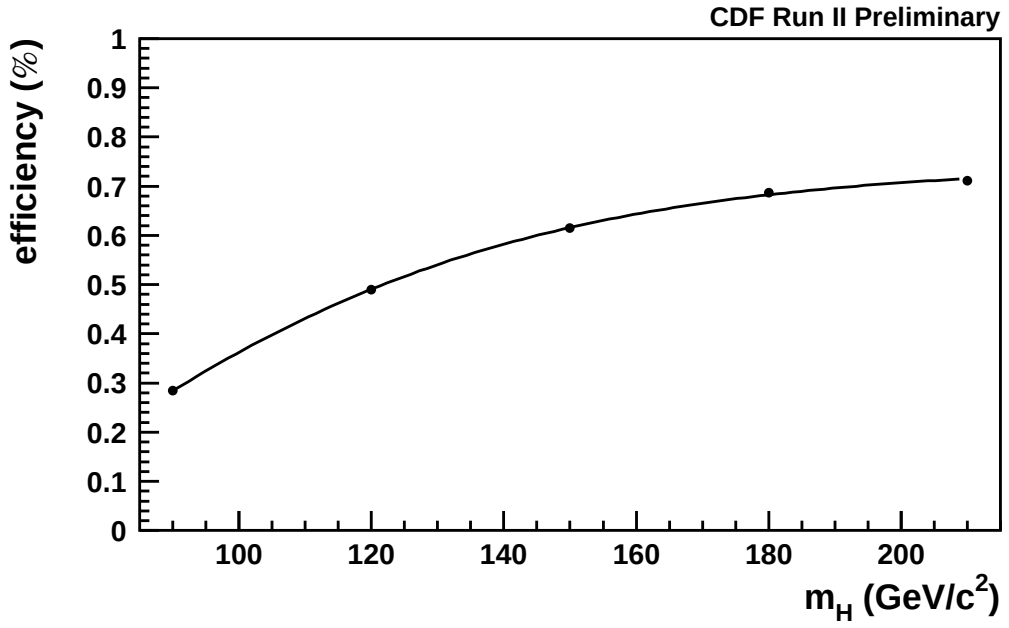

The associated b quarks are required to have $p_T > 15$ GeV/c and $|\eta| < 2.5$ in order to match the cross sections reported by FeynHiggs [17] (which are derived from MCFM results [6]). The performance of the SECVTX algorithm in the Monte Carlo samples is calibrated to match the data using a procedure similar to that described in Ref. [15], modified to include the effects of the Level2 silicon tracking requirements. The efficiency of the trigger energy cluster matching is also corrected to match the data as a function of the jet E_T. The event selection efficiencies vary from 0.3% to 0.7% as a function of the mass of the Higgs boson and are shown in Figure 3.

The mass of the two leading jets in the event m_{12}, which use to separate signal from background in our fits, and the SECVTX tag mass combination m_{diff} are shown in Figure 4 for the five Higgs masses for which samples were generated. For intermediate mass points we derive distributions by histogram interpolation and estimate the selection efficiency using the parametrization shown in Figure 3.

III. BACKGROUNDS

The three-tag sample background is essentially all QCD heavy flavor multijet production. Other processes such as $t\bar{t}$ production and $Z \to b\bar{b}$ + jets were also considered but found to contribute at a negligible level. Using simulated samples of generic QCD multijet production produced with PYTHIA [16] to develop and test our methods, we find that virtually all of the QCD background in our selected triple-tag sample consists of events with at least two real b-tags, with the additional tag being any of a mistagged light jet, a c-tag, or another

FIG. 4: Distributions of m_{12} (top) and m_{diff} (bottom) for the Higgs signal samples, binned in the indicated increments. The lines simply connect the bin centers and do not represent parametrizations. All are normalized to unit area.

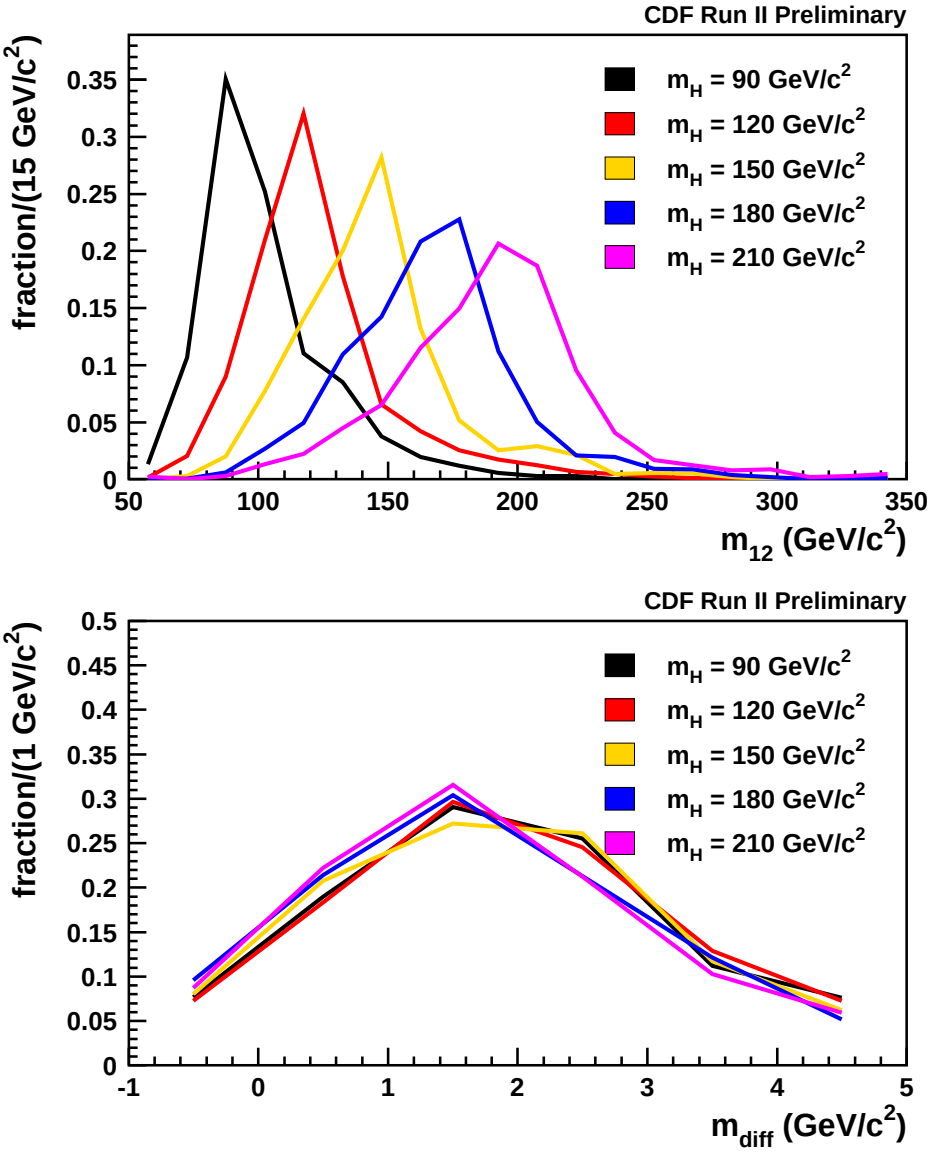

b-tag. The double-tagged three jet events are found to be predominantly two real b-tags, which makes them a natural starting point for constructing background estimates.

We describe the flavor structure of the jets in the event in the form XXY, where XX is the flavor of the two leading jets (i.e. bq would mean a b-jet (b) and a mistagged light quark (or gluon) jet (q)), while Y is the flavor of the third-leading jet. We make no distinction between the leading and second-leading jets, so that in a bcb event the charm tag could be either of the two leading jets. Under this convention we identify five types of event with at

FIG. 5: Distributions of m_{12} (top) and m_{diff} (bottom) for the background fit templates, binned in the indicated increments. The lines simply connect the bin centers and do not represent parametrizations. All are normalized to unit area.

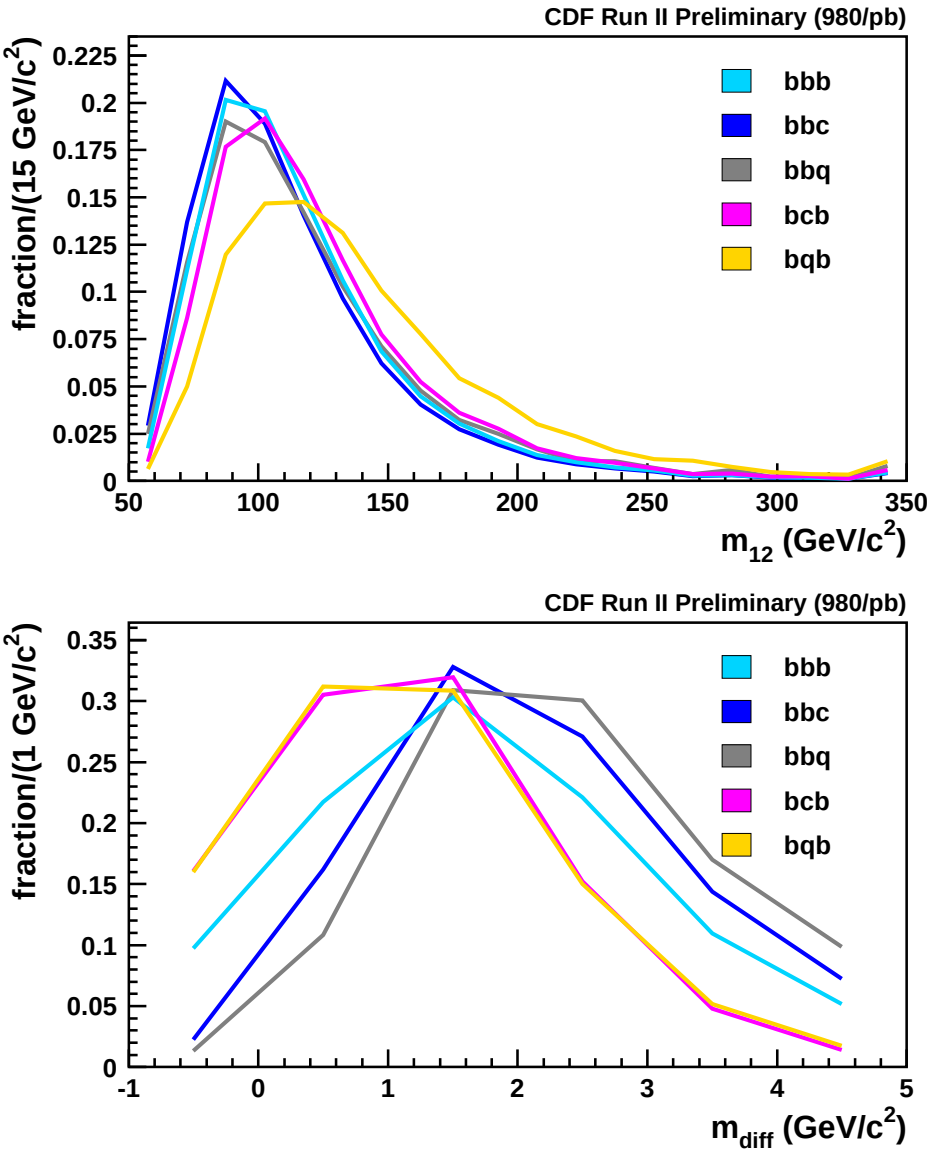

least two real b-tags. Three involve b-tags on both of the leading jets: *bbb*, *bbc*, and *bbq*. The other two, *bcb* and *bqb*, have the non-b-tag in one of the two leading jets. The templates we use in our fits for each of these components are shown in Figure 5. Descriptions of our methods for producing these templates follow.

A. General procedure

As noted above, the events with the two leading jets tagged and a third jet were found to almost always contain two real b-tags. This makes them an excellent starting point for constructing estimates of the *bbb*, *bbc*, and *bbq* backgrounds. In order to turn these double-tagged events into estimates of the triple-tagged sample we must simulate the effect of tagging the third jet. This is done using parametrizations of the SECVTX tag efficiency derived from large samples of simulated b, c, and light-flavor jets. The tag efficiencies are parametrized as a function of the jet E_T and the number of tracks in the jet passing the SECVTX quality cuts (but with no impact parameter requirement). The parametrizations also give a probability density for the SECVTX tag mass for a jet, defined as the mass of the tracks assigned to the displaced vertex. These tag masses are combined to produce a second discriminating variable alongside m_{12} as described below.

B. The *bbc* and *bbq* backgrounds

Starting from the double-tagged sample which we call bbj, where j means an untagged third jet, we weight the events by the probability to tag the third jet if it were a c-jet or a light jet to produce estimates for the shapes of the *bbc* and *bbq* background components, respectively. We float these components in an unconstrained fit to the data, so it is not necessary to know how many of the third jets are actually of each flavor, only to get the shapes of the m_{12} and m_{diff} distributions correct. Because there is a positive correlation between all of the jet energies, weighting the third jet as if it were mistagged will bias m_{12} towards higher values than in the *bbc* cases, because the light jet mistag rate rises much more quickly with growing jet E_T than does the c-tag efficiency. This effect can be seen by comparing the *bbc* and *bbq* distributions shown in Figure 5.

C. The *bbb* background

The third-jet weighting procedure works very well for *bbc* and *bbq* backgrounds, because the b-quark production physics is the same as in the bbj events used as the starting point. For the *bbb* background this is not the case. In bbj events there is a contribution from events with a gluon splitting into a $b\bar{b}$ pair, with those two b-jets representing the two leading jets. We find that in these events the two lead jets are less back-to-back than in events where the $b\bar{b}$ are produced directly in the hard scattering process, and therefore have a softer m_{12} distribution. More information on angular correlations in $b\bar{b}$ events and their relation to the various production mechanisms can be found in Ref. [18].

In *bbb* events, PYTHIA indicates that although there is still a sizeable contribution from $b\bar{b}$ pairs produced through gluon splitting, there must be two such splittings in the event and there is no reason why the two lead jets have to come from the same gluon. In fact we find no significant differences in the m_{12} spectra for *bbb* events between the different heavy flavor production mechanisms because of this ability to almost always choose a back-to-back pair. From very large generator-level PYTHIA samples we derive a correction function to map the m_{12} distribution of bbj events into one appropriate for *bbb*. We calibrate the PYTHIA bbj

sample to match the results in Table II of Ref. [18] (the "high ISR" row) by scaling up the gluon splitting contribution by a factor of two relative to the other mechanisms. The effect of this correction can be seen by comparing the m_{12} distributions of *bbb* and *bbc* in Figure 5, which would otherwise be essentially identical. Variation of the scale factor applied to the gluon splitting component of *bbj* is the most important systematic error on the background modeling.

D. The *bcb* background

The *bcb* background is similar to *bbb*, with the only difference being the *c*-tag in one of the two leading jets. The charm tag efficiency, while substaintially lower than for *b*-jets, has similar turn-on behavior versus jet E_T and therefore we expect that the m_{12} distribution in our *bbj* sample is a good estimate for what *bcj* would look like (except for the gluon splitting caveat discussed above). Therefore, we simply correct the SECVTX tag masses of the two leading jets in the *bbj* sample to make a distribution appropriate for *bcj*, using a correction function derived from Monte Carlo simulation. The gluon splitting effect is similar but larger for *bcb* than for *bbb*, because in *bcb* it is explicitly impossible to have the two leading jets come from the same gluon. The effect can be seen in Figure 5, again using *bbc* as a no-correction reference. Neglecting the m_{12} corrections applied to the double-tagged events when forming the *bbb* and *bcb* background templates would bias the Higgs signal fits by greater than the estimated statistical errors, so it is an important effect.

E. The *bqb* background

The last background shape is *bqb*, with two *b*-tags and one mistag that occurs in either of the two leading jets. Ideally we would start from a sample with one *b*-tag and one mistag and weight the third jet as a *b*-tag, however we do not know of a way to select such a sample in the data. Instead, we start from events with a tagged third jet and either of the two leading jets also tagged, and weight using a light jet mistag efficiency parametrization on the untagged jet (also prediciting its SECVTX tag mass). This has the undesirable feature of relying on predictions rather than observed tags in the two lead jets which have much more effect on m_{12} than does the third jet, however we expect this background to be small.

F. Backgrounds summary

The full set of background fit templates is shown in Figure 5. The backgrounds with two heavy flavor tags in the leading jet pair have similar m_{12} distributions, while *bqb* displays a harder spectrum due to the mistag bias. The backgrounds separate into three groups in the m_{diff} view, with *bbc* and *bbq* exhibiting the hardest spectra, *bcb* and *bqb* the softest, and *bbb* (and the Higgs signal) lying in between. For all background types we do not attempt to predict any absolute normalization. Instead, we float each component in the fit and let the data tell us how much of each type is present in our sample.

TABLE I: Summary of systematic uncertainties (for $m_H = 150$ GeV/c^2).

parameter	type	variation	applies to
luminosity	rate	±6%	signal
Monte Carlo statistics	rate	±3%	signal
selection efficiency	rate	±12.5%	signal
PDFs	rate	±8%	signal
jet energy scale	shape	±3%	signal
SECVTX tag mass modeling	shape	±3%	signal
bbq vs *bbc*	shape	full range	backgrounds
PYTHIA $g \to b\bar{b}$ rate scale factor	shape	2 ± 1	backgrounds

IV. SYSTEMATIC UNCERTAINTIES

Several sources of systematic uncertainty on the signal and background contributions were considered. These can take the form of uncertainties on the signal rate, or on the shapes of the fit templates. A summary is shown in Table I for $m_H = 150$ GeV/c^2. Shape uncertainties are introduced by modifying the templates used when throwing pseudoexperiments using an interpolation procedure, then fitting that modified pseudodata using the original default templates.

Rate uncertainties on the signal contribution relate to the number of events expected for a given cross section. They include the integrated luminosity of the data sample, the statistical errors due to the finite size of the generated signal samples, the efficiency of the trigger and SECVTX tagging requirements, and the effect on the efficiency due to uncertainties on PDFs. The selection efficiency uncertainty depends upon the Higgs mass, and varies from 11-17% over the mass range 90-210 GeV/c^2.

Shape uncertainties are applied to the corrections used for jet energy scale and SECVTX tag mass modeling to match the data. Of all these, the jet energy scale is the most significant source of uncertainty, particularly for Higgs masses below 120 GeV/c^2. As can be seen by comparing Figures 4 and 5, there is not a lot of difference between the m_{12} distributions for a low-mass Higgs and the background templates. The signal templates are more sharply peaked, however if the jet energy scale variation in a particular pseudoexperiment is large enough to move the peak in the pseudodata far from the peak in the default fit template, the fit is likely to ascribe many of the signal events in the pseudodata to one of the background templates instead of the signal, reducing the sensitivity. For higher Higgs masses the templates are less sharply peaked and not so similar to the background templates, so the loss in sensitivity is much less severe there.

The background templates float freely in the fit, so only shape uncertainties are considered. The *bbq* and *bbc* templates are too similar for the fit to constrain them both, so we use an average of the two as our default and interpolate between them to estimate a systematic uncertainty. The uncertainty on the calibration of the gluon splitting rate in PYTHIA applies to the *bbb* and *bcb* templates, and is the more important of the two sources.

FIG. 6: Fit of the triple-tagged data sample using only the QCD background templates.

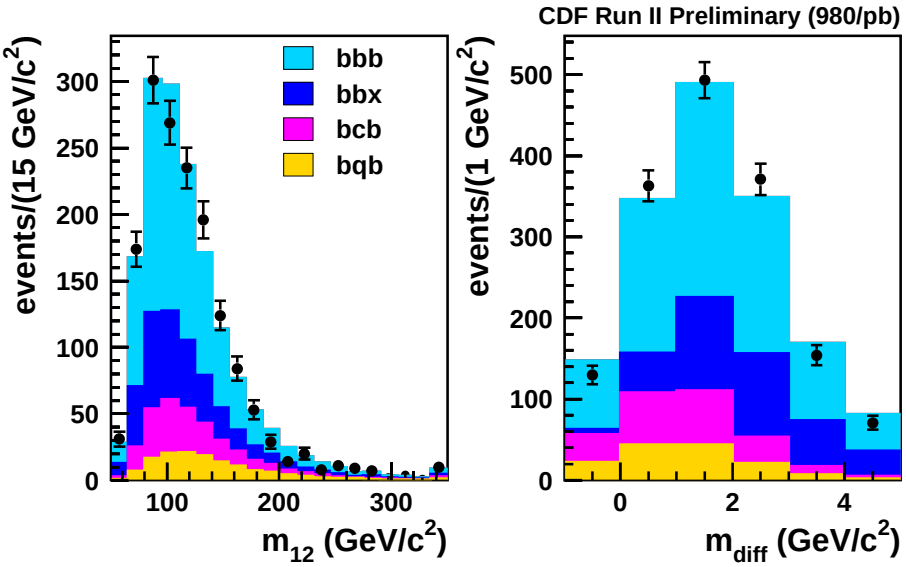

V. RESULTS

We begin with some simple fits of the data to show how the backgound templates work together, and conpare the results to predictions from PYTHIA. We also perform a fit with a signal template included for illustration. We move on to cross section times branching ratio limits for $bH, H \to b\bar{b}$ production in the case of a narrow standard model-like Higgs. Finally, we interpret our results as limits on $\tan\beta$ in the MSSM as a function of the pseudoscalar Higgs mass m_A, including the effects of the Higgs width.

A. Simple fits of the data

Figure 6 shows the result of a fit of the 1582 triple-tagged events observed in the data using the background templates only and with no systematic errors on the templates. We use a binned maximum-likelihood fit of two-dimensional templates in m_{12} versus m_{diff}, only the projections onto each axis are shown in Figure 6 are shown for clarity. The *bbx* component is the average of *bbq* and *bbc* as discussed in the previous section. The χ^2 between the observed data and predicted background is 154 for 93 degrees of freedom (some bins in the data are empty). The numbers of fitted events for each background type are given in Table II and compared to predictions obtained from the simulated PYTHIA multijet samples. The PYTHIA predictions are normalized to sum to the observed number of events in the data.

A sample fit including a template for a Higgs mass of 150 GeV/c^2 is shown in Figure 7; this mass exhibits the largest fitted signal contribution of the generated samples and is easiest to see on the plot. In this case the χ^2 is 143 for 92 degrees of freedom, with the fit assigning 80±40 events to the Higgs signal template. Because the m_{diff} variable cannot separate *bcb*

TABLE II: Numbers of fitted events for each background type and the PYTHIA predictions. The errors are statistical only.

background type	N_{fit}	PYTHIA prediction
bbb	762 ± 131	758
bbx	415 ± 82	325
bcb	279 ± 114	276
bqb	125 ± 82	222

FIG. 7: Fit of the triple-tagged data sample using the QCD background templates and one for $m_H = 150$ GeV/c^2.

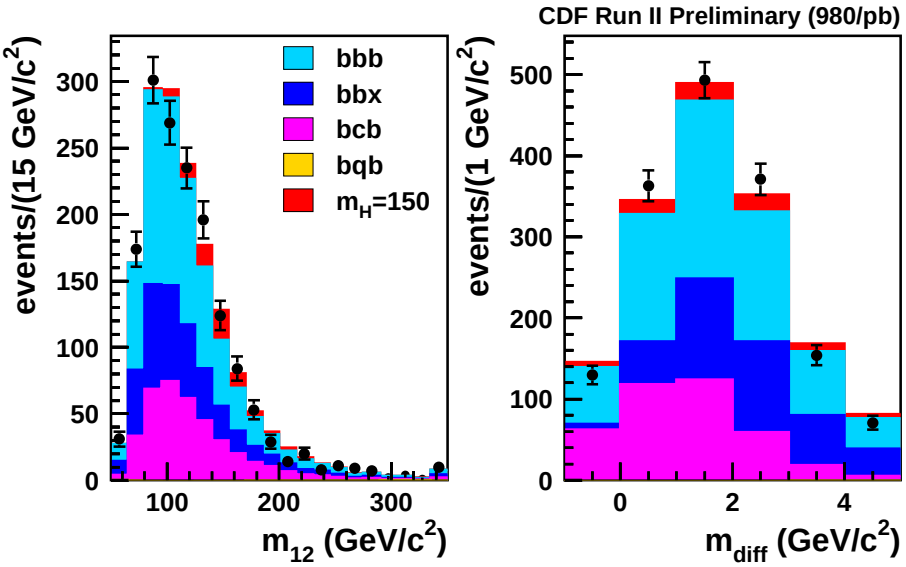

from bqb (see Figure 5), the fit has the freedom to move events between the two categories in order to obtain the best fit of m_{12}, as seen here where the fit prefers more bcb than in the backgrounds-only fit and essentially zero bqb. However, the 80 events ascribed to signal do not all come from the "missing" bqb; if the bqb contribution is fixed to 125 events as in the backgrounds-only case the fit still assigns 60 events to the Higgs signal template.

B. Cross section times branching ratio limits

The limit calculations were performed using the MCLIMIT package [19]. It performs the fitting to either the observed distribution or to pseudoexperiments, and calculates confidence levels using the CL_s method.

TABLE III: Median expected and observed limits on $\sigma(p\bar{p} \to bH) \times BR(H \to b\bar{b})$, in pb.

m_H	no systematics	bkgd systematics	full systematics	observed
90	72.1	70.9	144.7	141.6
100	63.3	72.5	133.9	109.3
110	37.9	48.6	69.5	65.7
120	23.4	29.6	39.4	43.4
130	20.3	25.7	30.2	46.6
140	16.5	20.3	23.6	40.9
150	12.7	14.5	17.9	31.4
160	12.1	13.4	15.4	23.9
170	10.7	11.4	13.1	16.6
180	8.7	9.1	11.3	9.5
190	8.3	8.5	9.7	7.3
200	7.3	7.3	8.3	5.0
210	6.0	6.0	7.3	3.5

Pseudoexperiments were generated using the results of the background-only fit in Figure 6. The background fractions and errors were used to determine how many of each type of event to generate in each pseudoexperiment. The nuisance parameters were set up to reproduce the anticorrelations as closely as possible, so that the total expected number of events in each pseudoexperiment was the same within 20-30 events. For pseudoexperiments that include Higgs signal, the expected signal fraction was subtracted from the background fractions in order to keep the average number of events constant.

The median expected limits on $\sigma \times BR$ for statistics only with no systematic errors, with only the variations on the background levels and shapes, and with the full systematics including variations on the signal level and shape are shown in Table III, along with the observed limits. Below 130 GeV/c^2 there is a considerable loss of senstivity due to systematics on the signal, primarily due to the jet energy scale variation as noted above. Above 130 GeV/c^2 this is less of an issue and the signal rate variations are relatively more important.

The expected and observed limits for the full systematics case are plotted as a function of the Higgs mass in Figure 8. Also shown are the bands resulting from calculating the expected limits using the $\pm 1\sigma$ and $\pm 2\sigma$ values of the test statistic from background-only pseudoexperiments. The most significant observed excess is at $m_H = 140$ GeV/c^2, with a p-value of 0.06. Using a trials factor of five estimated from the RMS of the signal m_{12} distributions, we expect to find an excess of this significance somewhere in the range 90-210 GeV/c^2 in around 30% of experiments.

C. MSSM interpretation

These limits can be trivially converted into limits on $\tan\beta$ versus the pseudoscalar mass m_A in MSSM models by diving by the standard model cross section times branching ratio

FIG. 8: Median, 1σ, and 2σ expected limits, and observed limits versus m_H on linear (top) and logarithmic (bottom) scales.

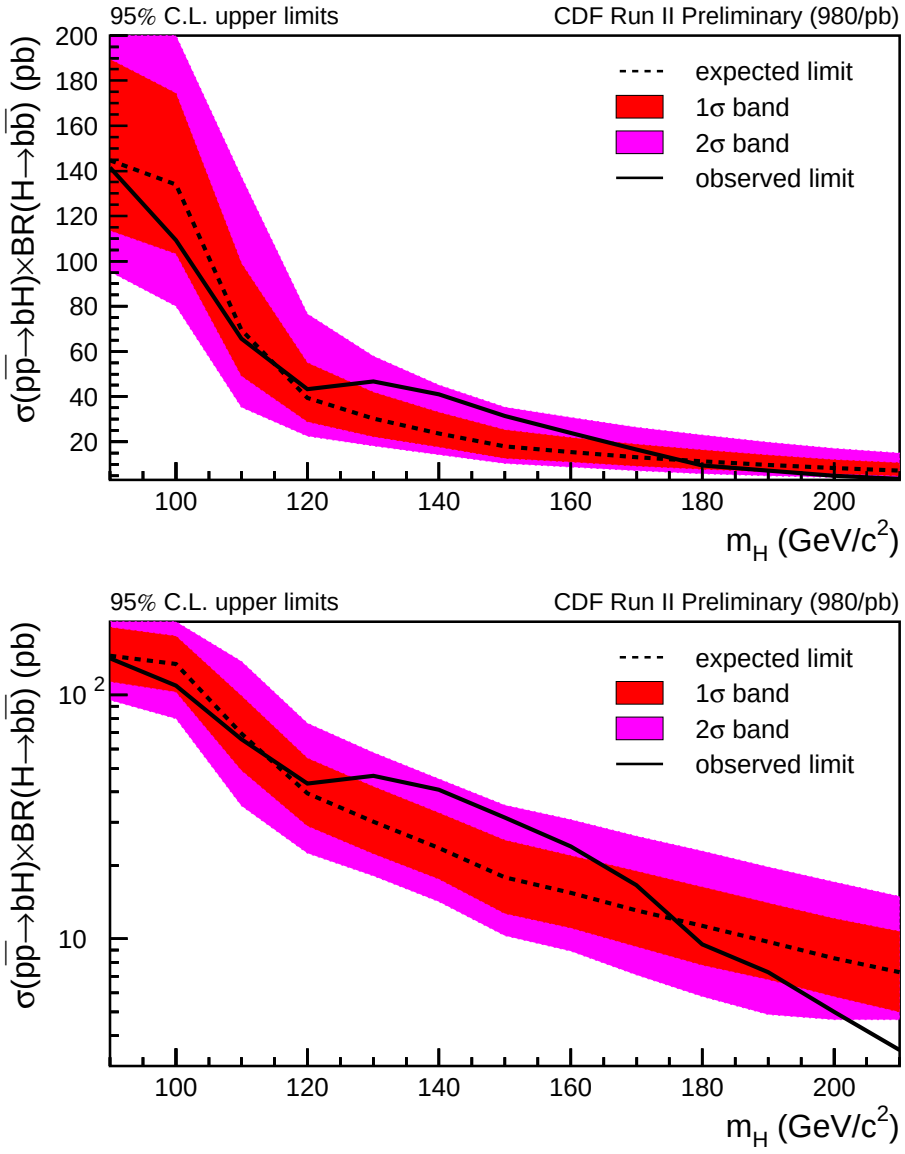

(90%) and taking the square root. The results of this are shown in Figure 9. The limits are not very realistic, however, because they do not include the effects of loop corrections which can enhance the cross section by more or less than $\tan^2\beta$ depending upon the MSSM scenario. They also do not include the effects of the Higgs width which can become significant when the down-type couplings are enhanced by such large factors.

Scaling the SM cross section by $\tan^2\beta$ is correct at tree level, however loop effects can modify this relationship and introduce dependence on other parameters of the MSSM. In Ref. [20] an approximate expression for the cross section times branching ratio is given as:

FIG. 9: Median, 1σ, and 2σ expected $\tan\beta$ limits (not including Higgs width effect or loop corrections), and the observed limits versus m_A.

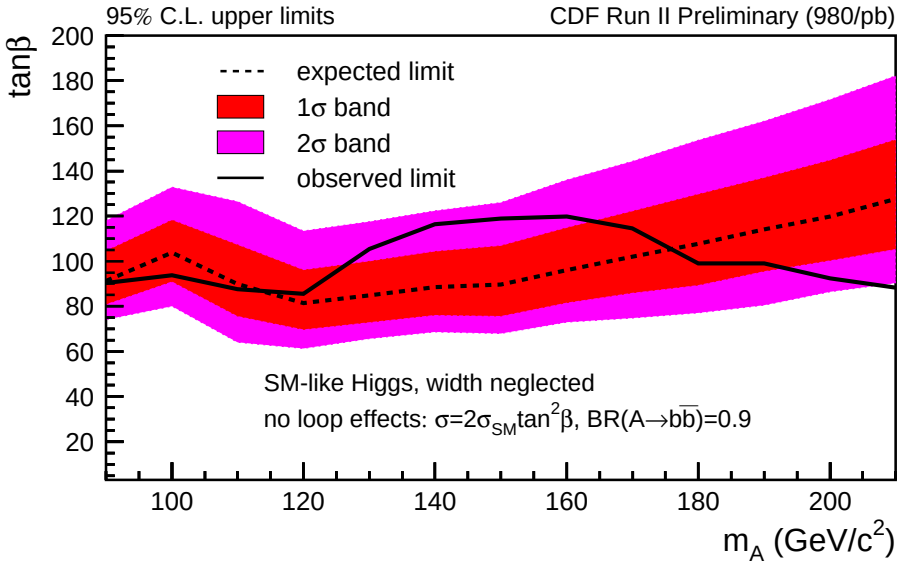

$$\sigma(b\bar{b}\phi) \times BR(A \to b\bar{b}) \simeq 2\sigma(b\bar{b}\phi)_{SM} \frac{\tan^2\beta}{(1+\Delta_b)^2} \times \frac{9}{(1+\Delta_b)^2+9} \quad (1)$$

where ϕ is a Higgs boson (either the SM variety or one of $h/H/A$), $\sigma(b\bar{b}\phi)_{SM}$ is the SM cross section, the factor of 2 comes from the degeneracy of A with either h or H, and the loop effects are incorporated into the Δ_b parameter. For our purposes it is important only to note that Δ_b is proportional to the product of $\tan\beta$ and the Higgsino mass parameter μ. Sample values of Δ_b given in Ref. [20] are -0.21 for the m_h^{max} scenario and -0.1 for the no-mixing scenario (at $\mu = -200$ GeV and $\tan\beta = 50$). It is apparent that negative values of μ and hence of Δ_b will increase the MSSM Higgs yield at fixed $\tan\beta$ above the tree level values and result in stronger limits on $\tan\beta$, while scenarios with μ positive will produce the opposite effect. Using Eqn. 1 we can predict the Higgs yield for any value of $\tan\beta$ and Δ_b and therefore derive limits in any desired scenario.

The limits shown in Figures 8 and 9 apply only to narrow Higgs like those in the standard model. If the cross section is increased by scaling the $b\bar{b}H$ coupling, as happens in the MSSM, then the width of the Higgs will increase as well. In order to account for this we used PYTHIA to produce m_H spectra for various values of the Higgs pole mass, $\tan\beta$, and Δ_b. Process 3 was used ($b\bar{b} \to H$) for this purpose, as process 32 which was used for the template samples does not properly take into account the $\hat{s}$-dependence of the width in the Breit-Wigner. The couplings to down-type quarks were scaled by $\tan\beta/(1+\Delta_b)$, to leptons (i.e. taus) by $\tan\beta$ (no loop effects here), and to up-type quarks and W/Z by zero. The initial state was forced to $b\bar{b}$ and no particular decay mode was selected in order for PYTHIA to report the full cross section. At least one of the b's accompanying the Higgs was required to have $p_T > 15$ GeV/c, $|\eta| < 2.5$, just like for the standard MC samples. Because the acceptance drops to zero, no

FIG. 10: Distributions of m_{12} for varying $\tan\beta$ and $\Delta_b = 0$, for Higgs pole mass of 150 GeV/c^2. All are normalized to unit area.

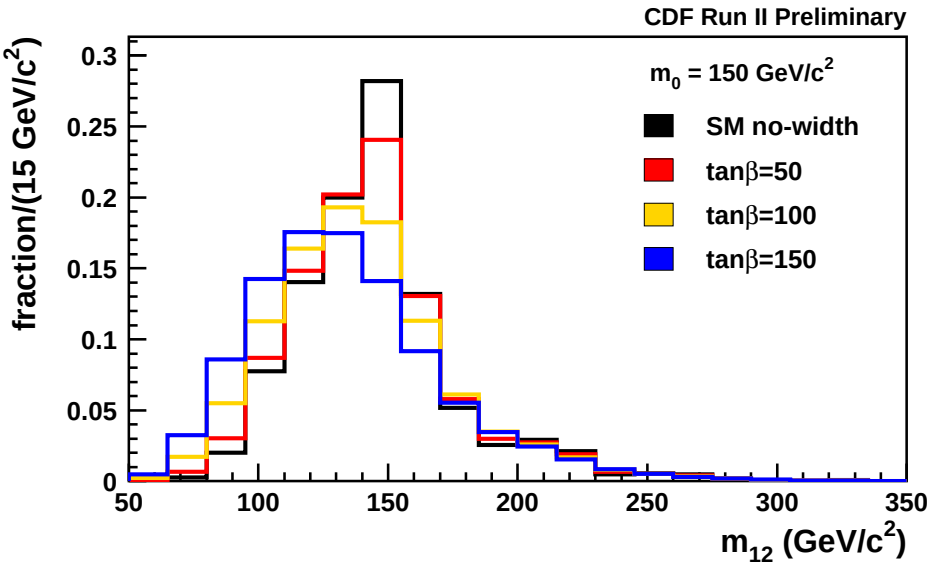

events were generated below $m_H = 57.5$ Gev/c^2 in order not to rely on the PYTHIA cross section calculation in that region.

Changing the width of the Higgs also changes the total cross section as a function of the pole mass. The spectra derived from PYTHIA are divided by the PYTHIA cross section estimate for a Higgs with SM couplings and by $\tan^2\beta/(1+\Delta_b)^2$, to produce an enhancement factor. This factor ranges from 0.95-0.75 for pole mass of 90 GeV/c^2 to 1.05-1.40 for 180 GeV/c^2, for $\tan\beta$ from 40-150. The factor drops below 1 for low pole mass because of the cutoff at 57.5 GeV/c^2. This information is needed when computing the expected number of events for a given Higgs mass and $\tan\beta$ value in the limits calculator.

Fit templates as a function of $\tan\beta$ were constructed by combining the narrow-width templates, weighted by the scaled m_H spectra obtained from PYTHIA and by the acceptance parametrization shown in Figure 3. An example is shown in Figure 10.

We scan in $\tan\beta$ from 40 to 200 in steps of 5 and calculate CL_s at each point, and exclude regions with $CL_s > 0.05$. The limits obtained are shown in Figure 11 for $\Delta_b = 0$. The limits get weaker in a highly $\tan\beta$-dependent way, so that compared with Figure 9 the -2σ contour moves much less than the $+2\sigma$ one does. This is because as $\tan\beta$ increases, the growing width spreads the events out over a larger region of m_{12}, reducing the fit power, and also tends to reduce the number of expected events due to the cross section lineshape extending downwards into regions with low or no acceptance. As the analysis is updated with more data in the future this effect should be less significant when the exclusion region moves into lower $\tan\beta$ regions.

To illustrate why the limits worsen so quickly at high $\tan\beta$, Figure 12 shows the result of a simple fit of the data similar to what was shown in Figure 7, except the signal template includes the width effects. As shown in Figure 10, the net effect is for the signal to spread

FIG. 11: Median, 1σ, and 2σ expected limits, and the observed limits versus m_A, including the Higgs width and for $\Delta_b = 0$.

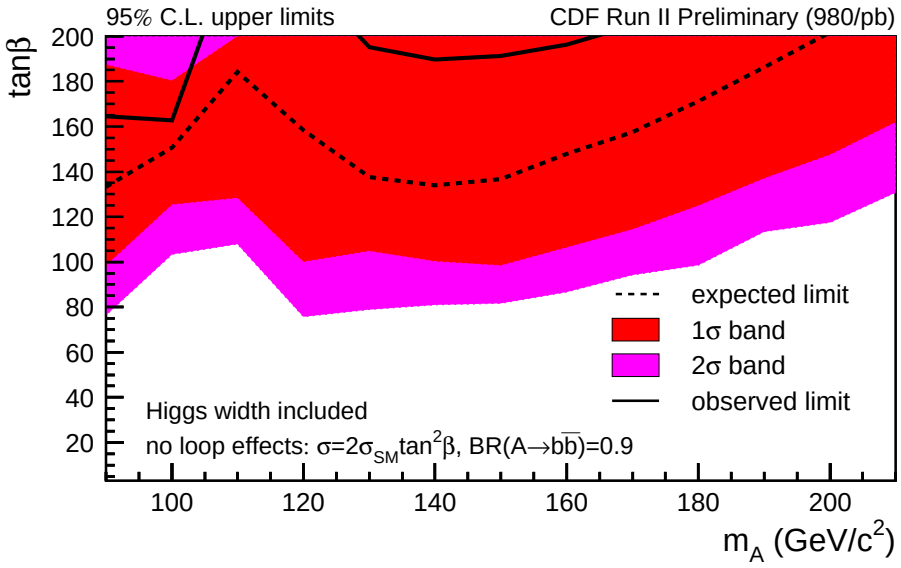

out into more bins, and also to shift towards lower values of m_{12} where the backgrounds are larger. Both of these effects reduce the statistical sensitivity of the search and require adding more signal to reach CL_s of 0.05, however that additional signal (i.e. higher $\tan\beta$) further broadens and shifts the m_{12} distribution, and so on.

Along with the $\Delta_b = 0$ case, limits were also generated for the m_h^{max} scenario with $\mu = -200$ GeV and are shown in Figure 13. Because of the relatively large and negative values of Δ_b in this scenario, the $\tan\beta$ limits are much tighter.

VI. CONCLUSION

A search for Higgs bosons produced in association with b-quarks was performed in 980 pb^{-1} of data. This process could be visible in supersymmetric models with high values of $\tan\beta$. The variable used was the mass of the two leading jets in triple-tagged events, with additional information from the SECVTX tag masses included to improve the background modeling.

The observed limits are within 2σ of expectations over the mass region from 90 to 210 GeV/c^2, with the largest excess occuring around 140 GeV/c^2. The results have been interpreted in two MSSM scenarios. In the case where loop effects are small, we find that the growth of the Higgs width as the couplings are enhanced permits only very weak limits on $\tan\beta$. In the m_h^{max} scenario with μ negative, the enhanced production through loop effects allows exclusion of $\tan\beta$ values greater than 80-120 over the mass range 90-210 GeV/c^2.

FIG. 12: Fit of the triple-tagged data sample using the QCD background templates and one for $m_H = 150$ GeV/c^2 with $\tan\beta = 150$ and $\Delta_b = 0$. Only the m_{12} projection is shown.

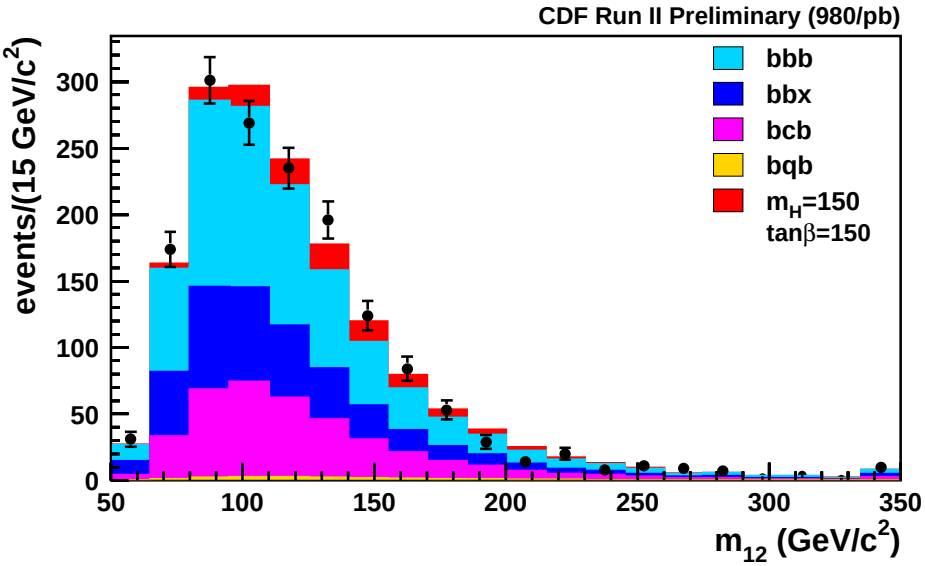

FIG. 13: Median, 1σ, and 2σ expected limits, and the observed limits versus m_H, including the Higgs width, for the m_h^{max} scenario with $\mu = -200$ GeV.

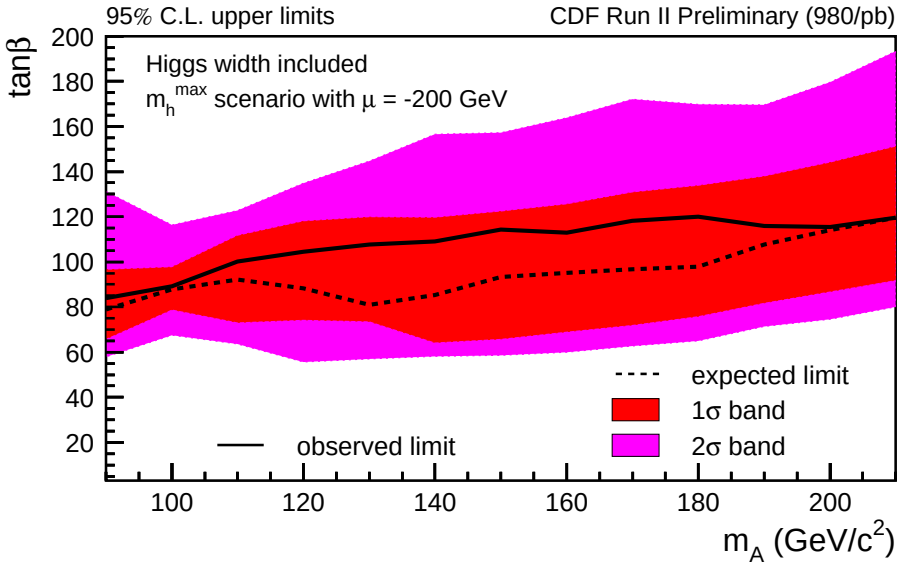

Acknowledgments

We thank the Fermilab staff and the technical staffs of the participating institutions for their vital contributions. This work was supported by the U.S. Department of Energy and National Science Foundation; the Italian Istituto Nazionale di Fisica Nucleare; the Ministry of Education, Culture, Sports, Science and Technology of Japan; the Natural Sciences and Engineering Research Council of Canada; the National Science Council of the Republic of China; the Swiss National Science Foundation; the A.P. Sloan Foundation; the Bundesministerium für Bildung und Forschung, Germany; the Korean Science and Engineering Foundation and the Korean Research Foundation; the Science and Technology Facilities Council and the Royal Society, UK; the Institut National de Physique Nucleaire et Physique des Particules/CNRS; the Russian Foundation for Basic Research; the Comisión Interministerial de Ciencia y Tecnología, Spain; the European Community's Human Potential Programme; the Slovak R&D Agency; and the Academy of Finland.

---

[1] M. Carena, S. Heinemeyer, C. E. M. Wagner, and G. Weiglein, "Suggestions for benchmark scenarios for MSSM Higgs boson searches at hadron colliders," *Eur. Phys. J.* **C26** (2003) 601–607, hep-ph/0202167.

[2] F. Maltoni. http://maltoni.home.cern.ch/maltoni/TeV4LHC/.

[3] R. V. Harlander and W. B. Kilgore, "Higgs boson production in bottom quark fusion at next-to- next-to-leading order," *Phys. Rev.* **D68** (2003) 013001, hep-ph/0304035.

[4] S. Dawson, C. B. Jackson, L. Reina, and D. Wackeroth, "Higgs production in association with bottom quarks at hadron colliders," hep-ph/0508293.

[5] S. Dawson, C. B. Jackson, L. Reina, and D. Wackeroth, "Hadronic Higgs Production with Heavy Quarks at the Tevatron and the LHC," hep-ph/0603112.

[6] J. Campbell, R. K. Ellis, F. Maltoni, and S. Willenbrock, "Higgs boson production in association with a single bottom quark," *Phys. Rev.* **D67** (2003) 095002, hep-ph/0204093.

[7] **DØ** Collaboration, V. M. Abazov *et al.*, "Search for neutral supersymmetric Higgs bosons in multijet events at $\sqrt{s} = 1.96$ TeV," *Phys. Rev. Lett.* **95** (2005) 151801, hep-ex/0504018.

[8] **DØ** Collaboration, "Search for Neutral Higgs Bosons at high $\tan\beta$ in Multijet Events," D0Note 5503-CONF. http://www-d0.fnal.gov/Run2Physics/WWW/results/prelim/HIGGS/H23/H23.pdf.

[9] **CDF** Collaboration, A. Abulencia *et al.*, "Search for neutral MSSM Higgs bosons decaying to tau pairs in $p\bar{p}$ collisions at $\sqrt{s} = 1.96$ TeV," *Phys. Rev. Lett.* **96** (2006) 011802, hep-ex/0508051.

[10] **CDF** Collaboration, "Search for Neutral MSSM Higgs Bosons Decaying to Tau Pairs," CDF Note 8676. http://http://www-cdf.fnal.gov/~aa/mssm_htt_1fb/note/cdf8676.pdf.

[11] **DØ** Collaboration, V. M. Abazov *et al.*, "Search for neutral Higgs bosons decaying to τ pairs in $p\bar{p}$ collisions at $\sqrt{s} = 1.96$ TeV," *Phys. Rev. Lett.* **97** (2006) 121802, hep-ex/0605009.

[12] **DØ** Collaboration, "Search for Neutral Higgs Boson Production in the Decay $h \to \tau_\mu \tau$ with the DØDetector at $\sqrt{s} = 1.96$ TeV," DØNote 5331-CONF. http://www-d0.fnal.gov/Run2Physics/WWW/results/prelim/HIGGS/H29/H29.pdf.

[13] **DØ** Collaboration, "Search for Neutral Higgs Bosons at high $\tan\beta$ in the $b(h/H/A) \to b\tau\tau$ Channel," DØNote XXXX-CONF.
http://www-d0.fnal.gov/Run2Physics/WWW/results/prelim/HIGGS/H24/H24.pdf.

[14] **CDF** Collaboration, D. Acosta *et al.*, "Measurement of the J/ψ meson and $b-$hadron production cross sections in $p\bar{p}$ collisions at $\sqrt{s} = 1960$ GeV," *Phys. Rev.* **D71** (2005) 032001, hep-ex/0412071.

[15] **CDF** Collaboration, "Measurement of the $t\bar{t}$ production cross section in $p\bar{p}$ collisions at $\sqrt{s} = 1.96$ TeV using Lepton+Jets Events with Secondary Vertex b-Tagging," CDF Note 8795.
http://www-cdf.fnal.gov/physics/new/top/confNotes/cdf8795_SecVtxXSPublic.ps.

[16] T. Sjostrand, S. Mrenna, and P. Skands, "PYTHIA 6.4 physics and manual," *JHEP* **05** (2006) 026, hep-ph/0603175.

[17] S. Heinemeyer *et al.* http://www.feynhiggs.de/.

[18] **CDF** Collaboration, D. Acosta *et al.*, "Measurements of $b\bar{b}$ azimuthal production correlations in $p\bar{p}$ collisions at $\sqrt{s} = 1.8$ TeV," *Phys. Rev.* **D71** (2005) 092001, hep-ex/0412006.

[19] T. Junk. http://www.hep.uiuc.edu/home/trj/cdfstats/mclimit_csm1/index.html.

[20] M. Carena, S. Heinemeyer, C. E. M. Wagner, and G. Weiglein, "MSSM Higgs boson searches at the Tevatron and the LHC: Impact of different benchmark scenarios," *Eur. Phys. J.* **C45** (2006) 797–814, hep-ph/0511023.